A Photoelectron Spectroscopic and Computational Study of Sodium Auride Clusters, $Na_nAu_n^-$ ($n = 1-3$)

Li-Feng Cui,[†] Ying-Chan Lin,[‡] Dage Sundholm,*[,‡] and Lai-Sheng Wang*[,†]

Department of Physics, Washington State University, 2710 University Drive, Richland, Washington 99354, Chemical & Materials Sciences Division, Pacific Northwest National Laboratory, MS K8-88, P. O. Box 999, Richland, Washington 99354, and Department of Chemistry, P.O. Box 55 (A.I. Virtanens plats 1), FIN-00014 University of Helsinki, Finland

Received: January 16, 2007; In Final Form: March 1, 2007

Negatively charged sodium auride clusters, $Na_nAu_n^-$ ($n = 1-3$), have been investigated experimentally using photoelectron spectroscopy and *ab initio* calculations. Well-resolved electronic transitions were observed in the photoelectron spectra of $Na_nAu_n^-$ ($n = 1-3$) at several photon energies. Very large band gaps were observed in the photoelectron spectra of the anion clusters, indicating that the corresponding neutral clusters are stable closed-shell species. Calculations show that the global minimum of $Na_2Au_2^-$ is a quasi-linear species with C_s symmetry. A planar isomer of D_{2h} symmetry is found to be 0.137 eV higher in energy. The two lowest energy isomers of $Na_3Au_3^-$ consist of three-dimensional structures of C_s symmetry. The global minimum of $Na_3Au_3^-$ has a bent-flake structure lying 0.077 eV below a more compact structure. The global minima of the sodium auride clusters are confirmed by the good agreement between the calculated electron detachment energies of the anions and the measured photoelectron spectra. The global minima of neutral Na_2Au_2 and Na_3Au_3 are found to possess higher symmetries with a planar four-membered ring (D_{2h}) and a six-membered ring (D_{3h}) structure, respectively. The chemical bonding in the sodium auride clusters is found to be highly ionic with Au acting as the electron acceptor.

1. Introduction

Relativistic effects cause the stabilization of the 6s orbital of gold, giving rise to its anomalously high electron affinity comparable to that of iodine.[1−6] Analogies between gold and halogens have been proposed because gold readily forms ionic alkali−Au compounds, in which Au acts as an electron acceptor.[7−9] Ever since the discovery of CsAu and RbAu in 1959,[10] stoichiometric alkali-gold compounds (M/Au = 1) have attracted particular attention. All of these compounds are stable, and their heat of formation decreases from LiAu to CsAu.[11] Proceeding through the series from LiAu to CsAu, a metal−insulator transition occurs between KAu and RbAu.[12] The insulating CsAu and RbAu crystallize in the cubic CsCl structure, whereas the structures of the metallic NaAu and KAu are more complicated and are still not fully elucidated.[10−15] Solid CsAu possesses an indirect band gap of 2.6 eV,[16] which can only be modeled when relativistic effects are included in band-structure calculations.[17,18] NaAu has been synthesized by precipitation from liquid ammonia solutions and observed in rapidly quenched alloys.[19−21] It has a metallic appearance and retains some gold color with the electrical conductivity lying in the metallic range.[10]

Some bimetallic gold−sodium clusters have been studied in the gas-phase previously.[22−26] Neutral sodium−gold Na_mAu_n clusters ($m = 0-10$, $n = 6-13$) were produced by Hoshino et al.,[22] who measured the ionization potentials of Na_mAu_n. Heiz et al.[23] investigated gold-doped alkali−metal clusters Na_nAu and Cs_nAu; they measured the ionization potentials of these clusters and performed theoretical calculations at the relativistic density-functional level. Their results indicated that the electronic structures of Na_nAu clusters are jelliumlike, whereas Cs_nAu clusters show significant ionic characters. The diatomics KAu and NaAu were studied using resonant two-photon ionization electronic spectroscopy by Duncan and co-workers,[24] who found ionic characters in both species.

We have been interested in the electronic structure and chemical bonding of bimetallic gold clusters both theoretically and experimentally using photoelectron spectroscopy (PES) of size-selected anions.[27−30] In Au−Si and Au−B mixed clusters, we found that a single gold atom can behave like a H atom to form fairly strong Au−Si or Au−B covalent bonds.[31−35] Very recently, we have combined PES and *ab initio* calculations on a series of sodium-coinage metal clusters of the form NaM_4^- (M = Cu, Ag, and Au) to determine their molecular structures and analyze their aromatic properties.[36] In the current work, we report a study of the finite-size analogs of the NaAu compound−free anionic and neutral stoichiometric Na_nAu_n ($n = 1-3$) clusters. The anionic $Na_nAu_n^-$ species were produced by laser vaporization and PES was used to probe their electronic properties. *Ab initio* calculations were carried out to elucidate the electronic and geometrical structures of both the anionic and neutral Na_nAu_n clusters for $n = 1-4$. Because the energy differences between the isomers are small, the interplay between experiment and theory is necessary for making the correct identification of the most stable isomers observed experimentally. The present studies on the sodium auride clusters may lead to further understanding of the electronic and structural properties of intermetallic compounds and liquid alloys, such as their ionicity and local order.[23,37]

* To whom correspondence should be addressed. E-mail: sundholm@chem.helsinki.fi (D.S.); ls.wang@pnl.gov (L.S.W.).

[†] Washington State University and Pacific Northwest National Laboratory.

[‡] University of Helsinki.

10.1021/jp0703511 CCC: $37.00
Published on Web 05/10/2007

2. Experimental and Computational Methods

2.1. Experimental Methods. The experiments were carried out using a magnetic-bottle PES spectrometer, details of which have been described before.[38,39] The gold−sodium alloy clusters were produced by laser vaporization of a compressed disk target made from Au and Na. The laser-produced plasma was mixed with a helium carrier gas pulse at 10 atm backing pressure. A cold cluster beam was produced by a supersonic expansion of the cluster-carrier gas mixture through a 2 mm diameter nozzle and collimated by a 6 mm diameter skimmer. The anions were extracted from the beam perpendicularly and separated by a time-of-flight mass spectrometer. Clusters with various Na and Au ratios were readily produced. For the stoichiometric $Na_nAu_n^-$ clusters, we were only able to observe significant mass signals for $n = 1-3$ with negligible signals for $n \geq 4$. The $Na_nAu_n^-$ cluster anions ($n = 1-3$) were each mass-selected and decelerated before crossing with a detachment laser beam in the interaction zone of the magnetic-bottle PES analyzer. In the current study, four photon energies were used: 532 nm (2.331 eV), 355 nm (3.496 eV), and 266 nm (4.661 eV) from a Nd:YG laser, and 193 nm (6.424 eV) from an ArF excimer laser. Photoelectrons were collected at nearly 100% efficiency by the magnetic-bottle and analyzed in a 3.5-m long electron flight tube. The spectra were calibrated with the known atomic species of Cu^-, Pt^-, and Au^-. The apparatus has an electron kinetic energy resolution ($\Delta E/E$) of ~2.5%, i.e., about 25 meV for 1 eV electrons.

2.2. Computational Methods. The molecular structures of the neutral and the anionic clusters were optimized at the second-order Møller-Plesset perturbation level (MP2) using the resolution-of-the-identity approach (RI).[40] The RI-MP2 calculations were performed with TURBOMOLE.[41] The stationary points obtained in the structure optimizations were checked by calculating the vibrational frequencies numerically using finite differences. For Na, the Karlsruhe standard triple-ζ valence basis sets augmented with double polarization functions (TZVPP) were used. For gold, we employed the Karlsruhe Au basis set consisting of 7s5p3d basis functions optimized for the neutral gold trimer[42,43] and augmented with 2f as suggested by Pyykkö et al.[44] For Au, the effective core potentials (ECP) from the Stuttgart group were employed.[45] The small-core ECP replaces 60 of the core electrons and thus 19 electrons per gold atom were considered in the calculations. In the correlation calculations, all considered electrons were correlated.

Theoretical photodetachment transitions were computed by adding excitation energies of the neutral clusters to the first vertical detachment energy (VDE) of the anionic clusters. The optimized molecular structures of the anions were used in the VDE calculations. The adiabatic detachment energies (ADEs) were calculated using the fully optimized structures of the neutral species. The singlet and triplet excitation energies were calculated with TURBOMOLE at the approximate coupled-cluster singles and doubles (CC2)[46] level using the RI approach.[47,48] The first VDE was calculated at the MP2 level as the difference in the total energy between the anionic and neutral species. Photodetachment transitions were also calculated for $NaAu^-$ and $Na_2Au_2^-$ at the coupled-cluster singles and doubles (CCSD) level using the equation-of-motion ionization-potential (EOMIP) formalism.[49] The coupled-cluster calculations were performed with the Austin-Mainz version of ACES II.[50] The same basis sets as used in the structure optimizations were employed in the EOMIP/CCSD calculations of the electronic detachment energies.

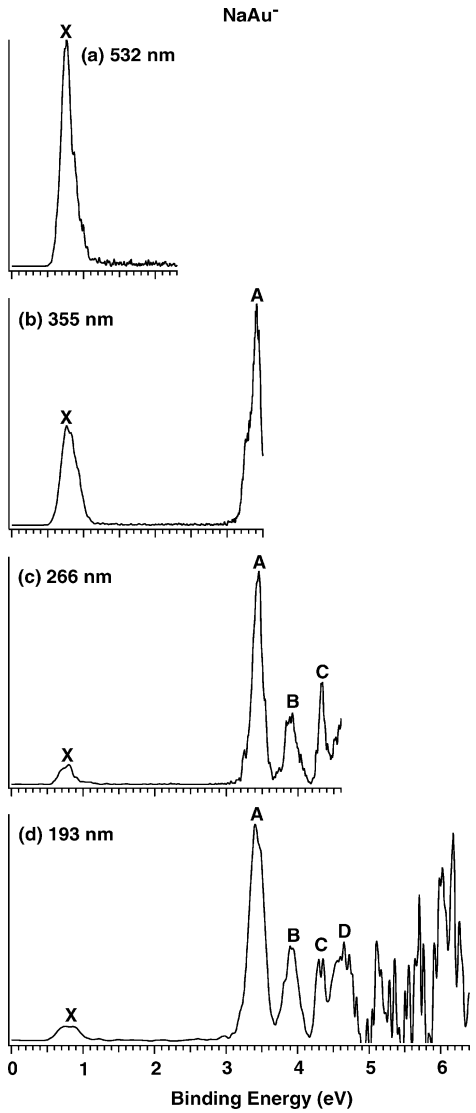

Figure 1. Photoelectron spectra of $NaAu^-$ measured at (a) 532 nm (2.331 eV), (b) 355 nm (3.496 eV), (c) 266 nm (4.661 eV), and (d) 193 nm (6.424 eV).

Because ordinary population analyses gave inconsistent atomic charge distributions, we used numerical integration to estimate the atomic charges. For the linear and quasi-linear isomers, numerical integration of the atomic charges was done as follows: a point along the Na−Au axis outside the Au atom was taken as the center of a sphere. The radius of the sphere was chosen such that the sphere surface cuts through the middle Na−Au bond. The radius of the sphere was kept fixed but the sphere center was adjusted along the Na−Au axis so that the Na−Au bond was cut in different points. The charge inside the sphere was integrated numerically. The inflection point of the obtained curve representing the number of electrons inside the sphere gave a good estimate of the charge of the gold atom. The same procedure was also used to determine the charge of the Na end atoms and of the Au−Na fragments in $Na_2Au_2^-$.

3. Experimental Results

3.1. $NaAu^-$. Figure 1 displays the photoelectron spectra of $NaAu^-$ at the four different photon energies. The 532 nm spectrum (Figure 1a) shows one relatively sharp band (X), which is broader than the instrumental resolution, suggesting it contains unresolved vibrational features. The relatively sharp onset of the X band yields an ADE of 0.62 ± 0.03 eV, which also

TABLE 1: Experimental ADE and VDE's of $NaAu^-$ ($C_{\infty v}$) Compared with the Calculated Values[a]

	experiment		calculation		
	ADE	VDE	ADE (MP2)	VDE (CC2/MP2)	VDE (CCSD)
X	0.62 ± 0.03	0.77 ± 0.03	0.650	0.714	0.659
A		3.42 ± 0.03		3.417 (T)	3.572
B		3.89 ± 0.03		3.906 (S)	
C		4.32 ± 0.03		4.281 (T) 4.363 (T) 4.389 (S)	
D		~4.6		4.527 (T) 4.552 (S) 4.587 (T)	

[a] VDE values were computed at the CC2/MP2 and EOMIP/CCSD levels. The singlet (S) and triplet (T) final states of NaAu were calculated at the RI-CC2 level using the $NaAu^-$ optimized structure. All energies are in eV.

represents the electron affinity (EA) of neutral NaAu. The band maximum defines a VDE of 0.77 ± 0.03 eV for the ground state transition. At 355 nm (Figure 1b), a new band (A) is observed at a VDE of 3.42 eV, which defines the first excited-state of neutral NaAu with an excitation of 2.65 eV above the ground state (X). The X-A energy separation also represents an approximate measure of the gap between the highest occupied molecular orbital (HOMO) and the lowest unoccupied molecular orbital (LUMO) of NaAu. At 266 nm (Figure 1c), two more bands (B and C) are observed at VDE's of 3.89 and 4.32 eV, respectively. The 193 nm spectrum (Figure 1d) reveals more transitions at higher binding energies, but they are less well-defined due to the poor signal-to-noise ratio. A band D is tentatively labeled for the sake of discussion. The ADE and VDE's are given in Table 1, where they are compared with theoretical calculations at different levels of theory.

3.2. $Na_2Au_2^-$. The photoelectron spectra of $Na_2Au_2^-$ are shown in Figure 2 at the four photon energies. Both the 532 and 355 nm spectra display only one relatively sharp band (X) for the ground state transition, yielding a VDE of 1.54 ± 0.03 eV and an ADE of 1.46 ± 0.03 eV. At 266 nm (Figure 2c), a band (A) is observed at a VDE of 4.37 eV, which represents the first excited-state of Na_2Au_2 with an excitation energy of 2.83 eV. At 193 nm, an intense and sharp band (B) is observed at a VDE of 4.76 eV. Weaker and almost continuous signals are observed between 5 and 6 eV in the 193 nm spectrum, suggesting a high density of electronic states in the higher binding energy region. Two bands (C and D) are labeled for the sake of discussion. The ADE and VDE's are given in Table 2, where they are compared with theoretical calculations. Very weak signals are visible around 0.5 eV in the 532 and 355 nm spectra, as well as around 3.6 eV in the 266 and 193 nm spectra (Figure 2). These weak signals can be due to either impurities or weakly populated low-lying isomers. As will be shown below in the theoretical calculations (Table 2), these weak signals are consistent with the calculated VDE's of a low-lying D_{2h} isomer.

3.3. $Na_3Au_3^-$. The spectra of $Na_3Au_3^-$ become broad and more complicated, as shown in Figure 3 at the four photon energies. The 532 nm spectrum (Figure 3a) exhibits two very broad bands, labeled X and X′ at VDE's of 1.20 and 1.81 eV, respectively. The ADE for band X is estimated to be 0.79 ± 0.06 eV. At 355 nm (Figure 3b), the band X′ becomes much weaker and it is almost negligible in the 266 and 193 nm spectra, suggesting that it is due to a weakly populated isomer. The 266 nm spectrum (Figure 3c) reveals two overlapping bands at VDE's of 4.03 eV (A) and 4.25 eV (B), which should come

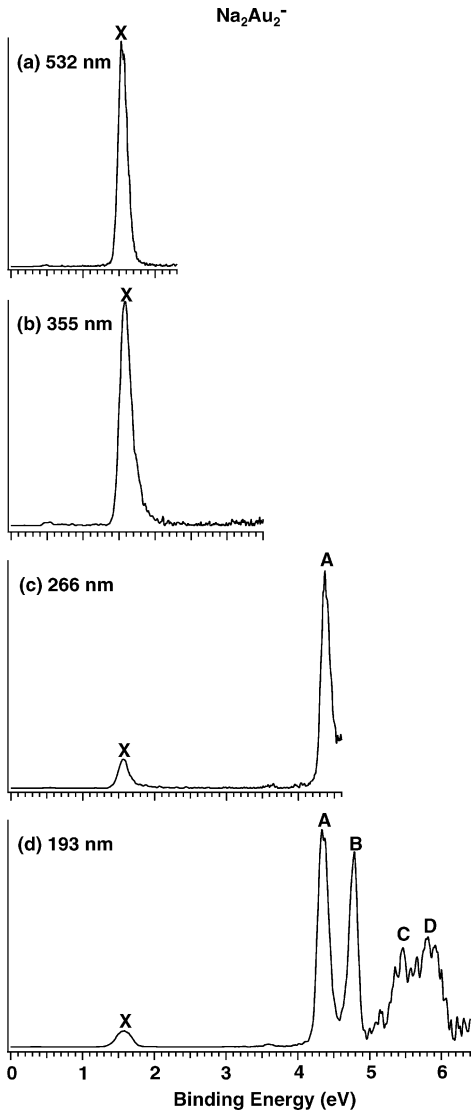

Figure 2. Photoelectron spectra of $Na_2Au_2^-$ measured at (a) 532 nm, (b) 355 nm, (c) 266 nm, and (d) 193 nm.

from the main isomer that gives rise to band X. The X−A energy separation of 2.83 eV defines a very large HOMO−LUMO gap for Na_3Au_3, similar to that in NaAu and Na_2Au_2. In the 193 nm spectrum (Figure 3d), more transitions are observed, which are not well resolved. Two broad bands (C and D) can be identified, which probably contain many overlapping detachment transitions. The observed ADE and VDE's are given in Table 3, where they are compared with theoretical calculations.

4. Theoretical Results

4.1. $NaAu^-$, NaAu, $Na_2Au_2^-$, and Na_2Au_2. The molecular structures of the anionic and neutral clusters were optimized at the RI-MP2 level, as described in Section 2.2. The Na−Au bond length in the neutral diatomic species is calculated to be 2.58 Å (Figure 4a), whereas that in the anion was found to increase to 2.75 Å (Figure 4b). The calculated VDE's from $NaAu^-$ are compared with the experiment in Table 1. For $Na_2Au_2^-$, we found two low-lying isomers: a quasi-linear structure of C_s symmetry (Figure 4d) and a rhombic structure of D_{2h} symmetry (Figure 4e). At the RI-MP2 level, the isomer of D_{2h} symmetry is 0.001 eV below the C_s one (Table 4). Electron correlation corrections obtained at the CCSD level shift the C_s isomer 0.137

TABLE 2: Experimental ADE and VDE's of $Na_2Au_2^-$ Compared with the Calculated Values[a]

	experiment		calculation			
			C_s		D_{2h}	
	ADE	VDE	VDE CC2/MP2	CCSD	ADE MP2	VDE CC2/MP2
X	1.46 ± 0.03	1.54 ± 0.03	1.536	1.465	0.284	0.298
A		4.37 ± 0.03	4.354 (T)	4.270		3.520 (T)
			4.401 (S)			3.902 (T)
B		4.76 ± 0.03	4.716 (T)	5.061		4.034 (S)
			4.837 (T)			4.108 (T)
C, D		~5−6	5.082 (T)	5.309		4.611 (T)
			5.145 (T)			4.651 (T)
			5.160 (S)			4.791 (T)
			5.186 (S)			4.720 (S)
			5.191 (T)			4.737 (T)
			5.200 (T)			4.818 (S)
			5.348 (S)			4.832 (S)
			5.388 (T)			4.835 (T)
			5.389 (S)			4.872 (S)
			5.390 (S)			4.891 (S)
			5.393 (T)			4.907 (T)
			5.444 (T)			
			5.458 (T)			
			5.516 (T)			
			5.555 (S)			
			5.570 (S)			
			5.650 (T)			
			5.651 (T)			
			5.679 (S)			
			5.680 (S)			
			5.698 (T)			

[a] VDE values were computed at the CC2/MP2 level. The singlet (S) and triplet (T) final states of Na_2Au_2 were calculated at the RI-CC2 level using the $Na_2Au_2^-$ optimized structures. For $Na_2Au_2^-$ (C_s), the VDEs were also calculated at EOMIP/CCSD level. All energies are in eV.

eV below the D_{2h} one; by adding the zero-point energy corrections the splitting increases to 0.162 eV. In the RI-MP2 optimization of neutral Na_2Au_2, only one low-lying isomer was obtained, namely a rhombic species of D_{2h} symmetry (Figure 4c). In the structural optimization of neutral Na_2Au_2 starting from the quasi-linear C_s structure of $Na_2Au_2^-$ (Figure 4d) the molecular structure relaxes without any barrier toward the rhombic structure. The VDE's have been calculated for both the C_s and D_{2h} isomers of $Na_2Au_2^-$, as given in Table 2. The molecular structures are reported as atomic coordinates in the Supporting Information.

4.2. $Na_3Au_3^-$ and Na_3Au_3. For $Na_3Au_3^-$, the two lowest energy isomers (Figure 4i and 4j) consist of three-dimensional structures of C_s symmetry. At the RI-MP2 level, the more compact structure (Figure 4j) is 0.022 eV lower in energy (Table 4), but by considering higher-order correlation effects at the CCSD level, the bent-flake structure (Figure 4i) is found to be 0.077 eV below the compact one. A quasi-linear isomer for $Na_3Au_3^-$ (Figure 4k) was also obtained, which was found to be 0.571 eV above the lowest isomer at the RI-MP2 level (Table 4). For neutral Na_3Au_3, the lowest energy isomer was found to be a six-membered ring of D_{3h} symmetry (Figure 4f). Another low-lying isomer (Figure 4g), which corresponds to the global minimum of the anion, lies only 0.089 eV higher in energy at the CCSD level. This isomer also possesses C_s symmetry, but is less bent. The compact isomer (Figure 4h) of Na_3Au_3 lies 0.140 eV above the D_{3h} structure at the CCSD level. The calculated ADE's and VDE's for the isomers of $Na_3Au_3^-$ are compared to the experimental data in Table 3.

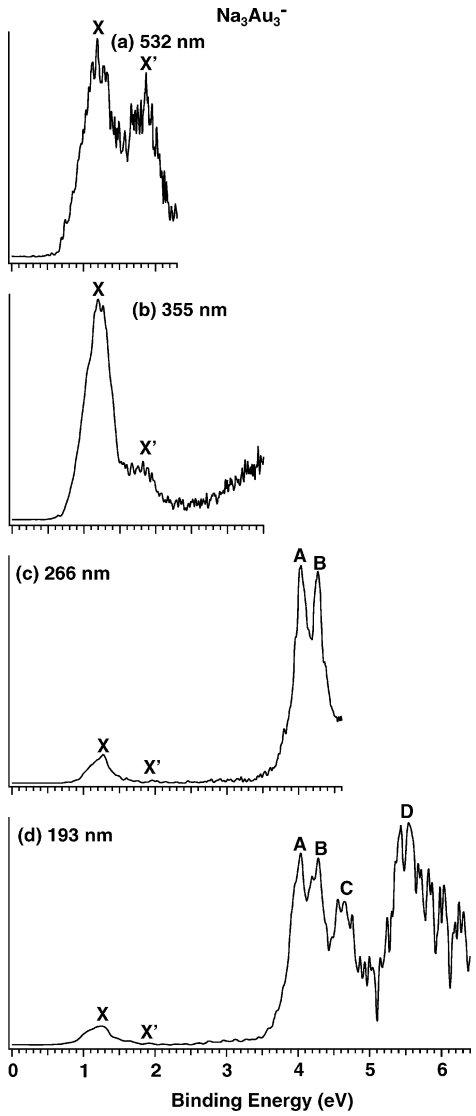

Figure 3. Photoelectron spectra of $Na_3Au_3^-$ measured at (a) 532 nm, (b) 355 nm, (c) 266 nm, and (d) 193 nm.

4.3. $Na_4Au_4^-$ and Na_4Au_4. The molecular structures were optimized for $Na_4Au_4^-$ and Na_4Au_4 even though the anionic species was not observed in the current experiment. The lowest energy isomer of the neutral Na_4Au_4 cluster is a distorted cube with T_d symmetry (Figure 4l), whereas for the anion there are three nearly degenerate isomers consisting of a slightly distorted tetrahedron of C_{3v} symmetry (Figure 4m) and two more irregular structures of C_1 symmetry (Figure 4n and 4o). Their relative energies at the RI-MP2 level are given in Table 4. The electron affinity for the Na_4Au_4 isomer with the T_d symmetry calculated at the RI-MP2 level is only 0.09 eV. The extremely low electron affinity indicates that the neutral cluster is very stable, but the anion would be very unstable, which might explain why $Na_4Au_4^-$ was not produced in the current experiment. The first VDE's for the C_{3v} and the two C_1 anionic clusters calculated at the RI-MP2 level are 0.34, 1.32 and 1.44 eV, respectively.

5. Discussion and PES Spectral Assignments

The VDE's of the energetically lowest $Na_nAu_n^-$ isomers were computed by adding CC2 singlet and triplet excitation energies of the neutral clusters to the first VDE of the anionic species calculated at the MP2 level. The characters of the first few

TABLE 3: Experimental ADE and VDE's of $Na_3Au_3^-$ Compared with the Calculated Values[a]

	experiment		calculation			
			C_s[b]		C_s[c]	
	ADE	VDE	ADE MP2	VDE CC2/MP2	ADE MP2	VDE CC2/MP2
X	0.79 ± 0.06	1.20 ± 0.05	0.696	1.138	0.631	0.885
X′		1.81 ± 0.05		1.862[d]		3.676 (T)
A		4.03 ± 0.03		4.023 (T)		3.989 (T)
B		4.25 ± 0.03		4.242 (T)		4.029 (S)
				4.342 (S)		4.255 (T)
C		4.61 ± 0.05		4.547 (S)		4.268 (S)
				4.684 (T)		4.348 (T)
				4.815 (T)		4.586 (T)
				4.827 (T)		4.615 (T)
				4.868 (T)		4.647 (S)
				4.956 (T)		
D		~5.4				

[a] VDE values were computed at the CC2/MP2 level. The singlet (S) and triplet (T) final states of Na_3Au_3 were calculated at the RI-CC2 level using the $Na_3Au_3^-$ optimized structures. All energies are in eV. [b] Bent-flake isomer of C_s symmetry (Figure 4i). [c] Compact isomer of C_s symmetry (Figure 4j). [d] From the quasi-linear isomer (Figure 4k).

excited states can be well described using single-electron transitions. The final states, electron configurations, and contribution percentage of the main electron configuration are given as Supporting Information (Tables S1−S3). For comparison with the experimental results, the VDE's were also calculated at the EOMIP/CCSD level for $NaAu^-$ and $Na_2Au_2^-$. The VDE's calculated at different levels are close to each other (Tables 1 and 2). The first few VDE's calculated at the EOMIP/CCSD level agree within 0.2 eV with the experimental values, whereas the values obtained at CC2/MP2 level are in excellent agreement with the experiment. Transitions to the excited states lying at 3.5 eV or higher above the ground state are originated from electron detachments of the 5d-derived molecular orbitals and are highly congested, consistent with experimental observations.

5.1. $NaAu^-$. The ground state electron configuration of $NaAu^-$ at the Hartree−Fock level is calculated to be $6\sigma^2 3\pi^4 1\delta^4 7\sigma^2 8\sigma^1$ ($^2\Sigma$), where the 8σ orbital corresponds to the LUMO of neutral NaAu and is antibonding mainly of Na 3s character, the 7σ orbital is a bonding orbital mainly of Au 6s character, and the 1δ, 3π, and 6σ orbitals are of Au 5d character. The first band X in the PES spectra (Figure 1) results from the detachment of the extra electron in the 8σ orbital, resulting in the ground state of NaAu ($^1\Sigma$). The Na−Au bond length is decreased from 2.75 Å in the anion to 2.58 Å in the neutral (Figure 4a and 4b), consistent with the antibonding nature of the 8σ orbital and the unresolved vibrational progression in the X band of the PES spectra (Figure 1). As seen in Table 1, the calculated ADE (0.650 eV) at MP2 level and the VDE (0.714 eV) at the CC2/MP2 level for the ground state transition are in good agreement with the experimental data, although the calculated VDE (0.659 eV) at the CCSD level appears to be slightly underestimated.

The next detachment channel is from the doubly occupied 7σ orbital, which yields both a triplet $^3\Sigma$ ($6\sigma^2 3\pi^4 1\delta^4 7\sigma^1 8\sigma^1$) and a singlet final state $^1\Sigma$ ($6\sigma^2 3\pi^4 1\delta^4 7\sigma^1 8\sigma^1$). The computed VDE's for these two states are in excellent agreement with the experimental values for bands A and B in the PES spectra, respectively (Table 1). Detachments from the Au 5d type orbitals lead to a complicated and congested set of excited states for neutral NaAu (Table 1), consistent with the less well resolved bands C and D. Overall, the calculated VDE's are in excellent agreement with the experimental data, verifying the validity of the theoretical methods for treating the Na−Au clusters.

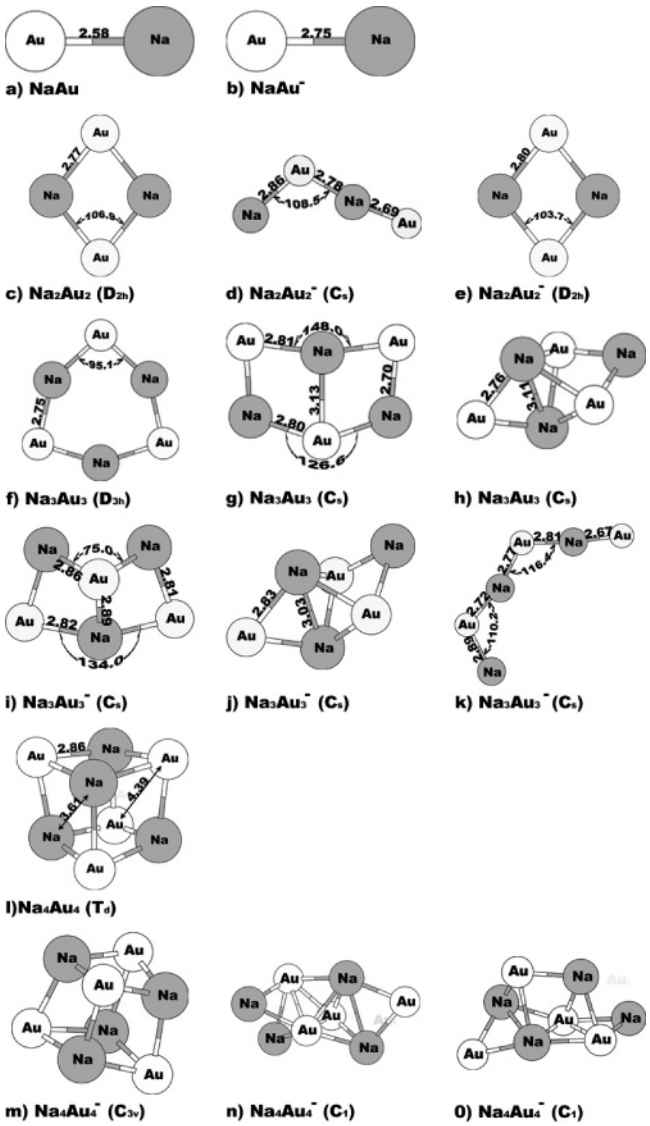

Figure 4. Molecular structures of Na_nAu_n and $Na_nAu_n^-$ ($n = 1-4$) optimized at the MP2 level. Selected bond lengths are in Å and the bond angles are in degrees.

TABLE 4: Relative Energies at RI-MP2 and CCSD Levels for Different Isomers of $Na_nAu_n^-$ and Na_nAu_n ($n = 2-4$) Presented in Figure 4[a]

isomers	RI-MP2	CCSD
$Na_2Au_2^-$ (d-C_s)	0	0
(e-D_{2h})	−0.001	0.137
$Na_3Au_3^-$ (i-C_s)	0	0
(j-C_s)	−0.022	0.077
(k-C_s)	0.571	–
Na_3Au_3 (f-D_{3h})	0	0
(g-C_s)	0.007	0.089
(h-C_s)	−0.079	0.140
$Na_4Au_4^-$ (m-C_{3v})	0	–
(n-C_1)	−0.006	–
(o-C_1)	0.086	–

[a] Total energies and atomic coordinates are given in Supporting Information. All energies are in eV.

5.2. $Na_2Au_2^-$. At the RI-MP2 level, the quasi-linear (C_s, Figure d) and the rhombic (D_{2h}, Figure 4d) $Na_2Au_2^-$ are almost degenerate, whereas at the CCSD level the C_s $Na_2Au_2^-$ is 0.137

eV lower in energy. The VDE calculated at the RI-MP2 level for the rhombic structure is only 0.298 eV, which is more than 1.2 eV smaller than the experimental value (Table 2). Therefore, the D_{2h} isomer can be firmly ruled out as the main $Na_2Au_2^-$ species observed experimentally. However, the low VDE for the D_{2h} isomer is consistent with the very weak signals observed around 0.5 eV (Figure 2a, b). Moreover, the calculated VDE for the second detachment channel for the D_{2h} isomer is 3.52 eV (Table 2), which is consistent with the weak feature at ~3.6 eV (Figure 2c, d). Thus, the D_{2h} isomer does seem to exist experimentally, albeit at very low abundance.

The calculated VDE for the C_s $Na_2Au_2^-$ at both the RI-MP2 (1.536 eV) and CCSD (1.465 eV) levels are in good agreement with the experimental value (Table 2), confirming unequivocally that the global minimum of $Na_2Au_2^-$ possesses the quasi-linear structure (Figure 4d). However, in our structural optimization for the neutral Na_2Au_2 starting from the C_s structure of $Na_2Au_2^-$, we found that it relaxes toward the rhombic D_{2h} structure, preventing us from computing the ADE for the C_s global minimum of $Na_2Au_2^-$. The ground state transition in the PES spectra of $Na_2Au_2^-$ yielded a fairly sharp band (X, Figure 2), suggesting that the C_s structure should be a local minimum on the potential energy surface of neutral Na_2Au_2. Perhaps, the energy barrier between the C_s and D_{2h} structures are too small in the neutral for us to locate the C_s minimum in our calculation.

The ground state electron configuration of the C_s $Na_2Au_2^-$ at the Hartree−Fock level is calculated to be $8a''^2 20a'^2 21a'^2 22a'^2 23a'^1$ ($^2A'$). The 23a′ orbital is primarily of Na 3s character, whereas the 22a′ and 21a′ orbitals are primarily of Au 6s character. Orbitals below 20a′ are all of Au 5d character. The first band X in the PES spectra results from the detachment of the extra electron in the 23a′ orbital. Detachment of an electron from the doubly occupied 22a′ orbital produces both a triplet and a single final state with calculated VDEs at 4.354 and 4.401 eV, respectively, at the RI-MP2 level (Tables 2 and S2), which are in excellent agreement with the experimental VDE of the A band (4.37 eV). The calculated VDE's for the triplet final states of removing an electron from the 21a′ and 20a′ orbitals are very close and should correspond to the well-resolved B band in the PES spectra (Table 2 and Figure 2). Beyond 5 eV, an extremely high density of electronic states from detachment of the Au 5d type orbitals is obtained (Table 2), consistent with the experimental observation of nearly continuous signals between 5 and 6 eV in the 193 nm spectrum (Figure 2d).

5.3. $Na_3Au_3^-$. The global minimum of $Na_3Au_3^-$ has a bent-flake structure of C_s symmetry (Figure 4i). The calculated ground state VDE from this anion is 1.138 eV at RI-MP2 level, in good agreement with the first VDE of the main isomer (1.20 ± 0.05 eV) observed experimentally (Table 3). The calculated ADE at RI-MP2 level for the bent-flake global minimum is 0.696 eV, consistent with the experimental value of 0.79 ± 0.06 eV. For the more compact $Na_3Au_3^-$ isomer (Figure 4j), the calculated first VDE at RI-MP2 level is 0.885 eV. If we examine the PES spectra carefully in Figure 3, there seem to be a shoulder on the leading edge of the X band, which could hint the presence of this more compact isomer, which is only 0.077 eV above the global minimum (Table 4). However, the overlap of this transition with the dominating transition (X) from the global minimum prevents us from a definitive assignment.

The extra band (X′) with a VDE of 1.81 eV observed more prominently in the 532 nm spectrum (Figure 3) must be due to another isomer, because no such VDE is obtained in the calculations from the two C_s isomers. The calculated first VDE from the quasi-linear isomer (Figure 4k) is 1.862 eV at RI-MP2 level, in excellent agreement with the X′ band. The quasi-linear isomer is a minimum on the potential-energy surface because no imaginary vibrational frequencies are obtained in the calculation. However, it is surprising that this isomer is present at all because it lies 0.571 eV above the global minimum at the RI-MP2 level (Table 4). The observation of the quasi-linear isomer of $Na_3Au_3^-$ may be understood from a kinetic point of view because it can be viewed as simply adding a NaAu unit to the quasi-linear $Na_2Au_2^-$ (Figure 4d). There may exist a significant barrier preventing the quasi-linear $Na_3Au_3^-$ from completely converting to the global minimum bent-flake structure. In any case, the 266 and 193 nm spectra (Figure 3) suggest that the presence of the higher energy isomers is negligible because the X band from the global minimum dominates in the low binding energy range. Therefore, the main features in the higher binding energy range observed in the 266 and 193 nm spectra should all primarily come from the bent-flake isomer.

The ground state electron configuration of the bent-flake global minimum of $Na_3Au_3^-$ (Figure 4i) at the Hartree−Fock level is calculated to be $18a''^2 25a'^2 19a''^2 26a'^2 27a'^1$ ($^2A'$), where the 27a′, 26a′, 19a″, and 25a′ are mainly of Au 6s and Na 3s characters, and the 18a″ orbital and deeper MO's are mainly due to the Au 5d. Detachment from the 27a′ orbital with a calculated VDE of 1.138 eV yields the ground state band (X) in the PES spectra of $Na_3Au_3^-$ (Tables 3 and S3). The second detachment channel is from the 26a′ orbital, which results in a triplet final state with a calculated VDE of 4.023 eV and a singlet final state with a calculated VDE of 4.342 eV (Table 3 and Table S3). The calculated VDE from the triplet final state is in excellent agreement with the VDE measured for the A band (4.03 eV), whereas the singlet state may contribute to the B band (VDE: 4.25 eV). The next detachment channel is from the 19a″ orbital, which also leads to a triplet and singlet final state with calculated VDE's of 4.242 and 4.547 eV, respectively (Tables 3 and S3). The calculated VDE for the triplet final state of this detachment channel is in excellent agreement with the measured VDE of the B and (4.25 eV), whereas the singlet final state is in good agreement with band C. Our calculations show that beyond 4.5 eV there is a high density of electronic states, consistent with the congested spectral features in the high binding energy side in the 193 nm spectrum (Figure 3).

5.4. Chemical Bonding in the Na_nAu_n and $Na_nAu_n^-$ Clusters. The excellent agreement between the theoretical calculations and the experimental PES data provide significant credence for the identified global minimum structures for the $Na_nAu_n^-$ and Na_nAu_n clusters. We note that the potential energy surfaces of the anions and the neutral are quite different for the $n = 2$ and 3 cases. Small sodium auride clusters are expected to have significant ionic characters because the electron affinity of gold is much larger than that of sodium. Our calculations suggest that Na and Au atoms in small neutral Na_nAu_n show significant ionic interactions and can be viewed as $(Na^+Au^-)_n$. For neutral NaAu, the numerical integration of the charge density shows that Na is positively charged with a net charge of about +0.7 |e|. Earlier studies on gold-alkali metal species also indicated that charge is transferred from the alkali metal to the gold atom.[23,24] The neutral Na_2Au_2 and Na_3Au_3 clusters adopt planar D_{2h} and D_{3h} ring structures and Na_4Au_4 possesses an almost cubic T_d structure, which are similar to those of the corresponding $(NaCl)_n$ clusters.[51] In the small anionic $Na_nAu_n^-$ clusters ($n = 1, 2$) the extra electron goes to the Na site and the sodium atoms remain practically neutral, whereas the extra charge is carried by the Au atoms. Addition of one extra electron

to Na_2Au_2 produces a Na−Au−Na−Au$^-$ quasi-linear structure. The Au atom at the end of the quasi-linear structure (Figure 4d) has a charge surplus of 0.3 electron and the net charge of the middle Au atom is −0.7 |e|. Our calculations show that $Na_3Au_3^-$ also has a low-lying quasi-linear isomer, which is observed experimentally and can be viewed as the extension of the global minimum of $Na_2Au_2^-$ by one NaAu unit.

6. Summary

Photoelectron spectroscopy has been combined with high-level *ab initio* calculations to examine the electronic and atomic structures of a series of stoichiometric sodium auride clusters, $Na_nAu_n^-$ ($n = 1-3$). Well-resolved photoelectron spectra have been obtained and are compared with *ab initio* calculations at several levels of sophistication to confirm the global minima of the anionic and neutral clusters. The lowest energy isomer of $Na_2Au_2^-$ was identified as a quasi-linear molecule of C_s symmetry. A planar isomer of D_{2h} symmetry lies 0.137 eV higher in energy. The two lowest energy isomers of $Na_3Au_3^-$ consist of three-dimensional structures of C_s symmetry. The energetically lowest one has a bent-flake structure and lies only 0.077 eV below a compact cluster structure of C_s symmetry. A quasi-linear isomer was also observed for $Na_3Au_3^-$ experimentally and was born out from our calculations. The potential energy surfaces for the neutral clusters are found to be quite different from that of the anions for Na_2Au_2 and Na_3Au_3. Molecular structure calculations of neutral Na_2Au_2 yielded a planar four-membered ring of D_{2h} symmetry. For neutral Na_3Au_3, the lowest energy isomer consists of a planar six-membered ring of D_{3h} symmetry.

Acknowledgment. The experimental work was supported by the U.S. National Science Foundation (CHE-0349426) and performed at the W.R. Wiley Environmental Molecular Sciences Laboratory, a national scientific user facility sponsored by the U.S. DOE's Office of Biological and Environmental Research and located at Pacific Northwest National Laboratory, operated for the DOE by Battelle. We thank Dr. Xi Li for help during the experiment. The theoretical research was supported by the Academy of Finland through its Centers of Excellence Program 2006-2011. We acknowledge financial support from the European research training network on "Understanding Nanomaterials from a Quantum Perspective" (NANOQUANT), contract No. MRTN-CT-2003-506842 and from the Nordisk Forskerakademi network for research and research training (NorFA grant No. 030262) on "Quantum Modeling of Molecular Materials" (QMMM). We also thank Prof. Ahlrichs (Karlsruhe) and Prof. Gauss (Mainz) for up-to-date versions of the TURBOMOLE and ACES II program packages.

Supporting Information Available: Atomic coordinates are given for the molecular structures of the $Na_nAu_n^-$ and Na_nAu_n species ($n = 1-4$) optimized at the RI-MP2 level using the TZVPP (Na) and 7*s*5*d*3*d*2*f* (Au) basis sets. Energies obtained at the MP2 and CCSD levels and the characters of the excited states are also reported in Tables S1−S3. This material is available free of charge via the Internet at http://pubs.acs.org

References and Notes

(1) Pyykkö, P. *Angew. Chem., Int. Ed.* **2004**, *43*, 4412.
(2) Schwarz, H. *Angew. Chem., Int. Ed.* **2003**, *42*, 4442.
(3) Schwerdtfeger, P. *Angew. Chem., Int. Ed.* **2003**, *42*, 1892.
(4) Schwerdtfeger, P. *Heteroat. Chem.* **2002**, *13*, 578.
(5) Schmidbaur, H. In *Gold. Progress in Chemistry, Biochemistry and Technology*; Wiley: Chichester, UK, 1999; p 894.
(6) Desclaux, J. P.; Pyykkö, P. *Chem. Phys. Lett.* **1976**, *39*, 300.
(7) Jansen, M.; Murding, A. V. In *Gold. Progress in Chemistry, Biochemistry and Technology*; Schmidbaur, H., Ed.; Wiley: New York, 1999; p 747.
(8) Pyykkö, P. *Angew. Chem., Int. Ed.* **2002**, *41*, 3573.
(9) Gagliardi, L. *J. Am. Chem. Soc.* **2003**, *125*, 7504.
(10) Spicer, W. E.; Sommer, A. H.; White, J. G. *Phys. Rev. Lett.* **1959**, *115*, 57.
(11) Koenig, C.; Dristensen, N. E.; Kollar, J. *Phys. Rev. B* **1984**, *29*, 6481.
(12) Kienast, G.; Verma, J. *Z. Anorg. Allg. Chem.* **1961**, *310*, 143.
(13) Zachwieja, U. *Z. Anorg. Allg. Chem.* **1993**, *619*, 1095.
(14) Krieger-Beck, P.; Brodbeck, A.; Strähle, J. *Z. Naturforsch.* **1989**, *44b*, 237.
(15) Batchelor, R. J.; Birchall, T.; Burns, R. C. *Inorg. Chem.* **1986**, *25*, 2009.
(16) Spricer, W. E. *Phys. Rev.* **1962**, *125*, 1297.
(17) Hasegawa, A.; Watabe, M. *J. Phys. F* **1977**, *7*, 75.
(18) Christensen, N. E.; Kollar, J. *Solid State Commun.* **1983**, *46*, 727.
(19) Pelton, A. D. *Bull. Alloy Phase Diagrams* **1986**, *7*, 136.
(20) Zintl, E.; Boubeau, J.; Dullenkopf, W. *Z. Phys. Chem.* **1931**, *A154*, 1.
(21) Haucke, W. *Z. Elektrochem.* **1937**, *43*, 712.
(22) Hoshino, K.; Naganuma, T.; Watanabe, K.; Nakajima, A.; Kaya, K. *Chem. Phys. Lett.* **1993**, *211*, 571.
(23) Heiz, U.; Vayloyan A.; Schumacher, E.; Yeretzian, C.; Stener, M.; Gisdakis, P.; Rösch, N. *J. Chem. Phys.* **1996**, *105*, 5574.
(24) Stangassinger, A.; Knight, A. M.; Duncan, M. A. *J. Phys. Chem. A* **1999**, *103*, 1547.
(25) Heiz, U.; Vayloyan, A.; Schumacher, E. *J. Phys. Chem.* **1996**, *100*, 15033.
(26) Baruah, T.; Blundell, S. A.; Zope, R. R. *Phys. Rev. A* **2001**, *64*, 043202.
(27) Li, X.; Kiran, B.; Li, J.; Zhai, H. J.; Wang, L. S. *Angew. Chem., Int. Ed.* **2002**, *41*, 4786.
(28) Zhai, H. J.; Kiran, B.; Wang, L. S. *J. Chem. Phys.* **2004**, *121*, 8231.
(29) Zhai, H. J.; Li, J.; Wang, L. S. *J. Chem. Phys.* **2004**, *121*, 8369.
(30) Li, X.; Kiran, B.; Cui, L. F.; Wang, L. S. *Phys. Rev. Lett.* **2005**, *95*, 253401.
(31) Kiran, B.; Li, X.; Zhai, H. J.; Cui, L. F.; Wang, L. S. *Angew. Chem., Int. Ed.* **2004**, *43*, 2125.
(32) Li, X.; Kiran, B.; Wang, L. S. *J. Phys. Chem. A* **2005**, *109*, 4366.
(33) Zhai, H. J.; Wang, L. S.; Zubarev, D. Y.; Boldyrev, A. I. *J. Phys. Chem. A* **2006**, *110*, 1689.
(34) Zubarev, D. Y.; Li, J.; Wang, L. S.; Boldyrev, A. I. *Inorg. Chem.* **2006**, *45*, 5269.
(35) Kiran, B.; Li, X.; Zhai, H. J.; Wang, L. S. *J. Chem. Phys.* **2006**, *125*, 133204.
(36) Lin, Y. C.; Jusélius, J.; Sundholm, D.; Cui, L. F.; Li, X.; Zhai, H. J.; Wang, L. S. *J. Phys. Chem. A* **2006**, *110*, 4244.
(37) Saboungi, M.-L.; Geertsma, W.; Price, D. L. *Annu. Rev. Phys. Chem.* **1990**, *41*, 207.
(38) Wang, L. S.; Cheng, H. S.; Fan, J. *J. Chem. Phys.* **1995**, *102*, 9480.
(39) Wang, L. S.; Wu, H. In *Advances in Metal and Semiconductor Clusters: Cluster Materials*; Duncan, M. A., Ed.; JAI Press: Greenwich, CT, 1998; pp 299−343.
(40) Weigend, F.; Häser, M. *Theoret. Chem. Acc.* **1997**, *97*, 331.
(41) Ahlrichs, R.; Bär, M.; Häser, M.; Horn, H.; Kölmel, C. *Chem. Phys. Letters* **1989**, 162, 165; See http://www.turbomole.de.
(42) Gilb, S.; Weis, P.; Furche, F.; Ahlrichs, R.; Kappes, M. M. *J. Chem. Phys.* **2002**, *116*, 4094.
(43) The optimized p exponent of 0.80896058156 was used. The exponents of the f functions were 1.19 and 0.43023309776.
(44) Pyykkö, P.; Runeberg, N.; Mendizabal, F. *Chem. Eur. J.* **1997**, *3*, 1451.
(45) Andrae, D.; Häussermann, U.; Dolg, M.; Stoll, H.; Preuss, H. *Theor. Chim. Acta* **1990**, *77*, 123.
(46) Christiansen, O.; Koch, H.; Jørgensen, P. *Chem. Phys. Lett.* **1995**, *243*, 4041.
(47) Hättig, C.; Weigend, F. *J. Chem. Phys.* **2000**, *113*, 5154.
(48) Weigend, F.; Häser, M.; Patzelt, H.; Ahlrichs, R. *Chem. Phys. Lett.* **1998**, *294*, 143.
(49) Stanton, J. F. *J. Chem. Phys.* **1994**, *101*, 8938.
(50) Stanton, J. F.; Gauss, J.; Watts, J. D.; Lauderdale, W. J.; Bartlett, R. J. *Intern. J. Quantum Chem. Symp.* **1992**, 26, 879; Stanton, J.; Gauss, J.; Watts, J. D.; Lauderdale, W. J.; Bartlett, R. J. *ACES II, an ab initio program system*, which includes modified versions of Almlöf, J.; Taylor, P. R. *MOLECULE Gaussian integral program*; Helgaker, T.; Jensen, H. J. Aa.; Jørgensen, P.; Taylor, P. R. *ABACUS integral derivative program* ; Taylor, P. R. *PROPS property integral code*. See http://www.aces2.de.
(51) Hargittai, M. *Chem. Rev.* **2000**, *100*, 2233.